



PII S0008-8846(96)00061-0

**RICE-HUSK ASH PASTE AND CONCRETE:  
SOME ASPECTS OF HYDRATION AND THE MICROSTRUCTURE OF THE  
INTERFACIAL ZONE BETWEEN THE AGGREGATE AND PASTE**

**M.H. Zhang\*, R. Lastra\*, and V.M. Malhotra\*\***

\*Research Scientists and \*\*Program Principal,  
CANMET, Natural Resources Canada, Ottawa, Canada

(Refereed)

(Received December 7, 1995; in final form March 22, 1996)

**ABSTRACT**

This paper presents an experimental study on the effects of the incorporation of rice-husk ash (RHA) in cement paste and concrete on the hydration and the microstructure of the interfacial zone between the aggregate and paste. The influence on the compressive strength of concrete is discussed, and the results are compared with those obtained with the control portland cement concrete and concrete incorporating silica fume. As for ordinary portland cement paste, it was found that calcium hydroxide  $[\text{Ca}(\text{OH})_2]$  and calcium silicate hydrates  $[\text{C-S-H}]$  were the major hydration and reaction products for the RHA paste. Because of the pozzolanic reaction, the paste incorporating RHA had lower  $\text{Ca}(\text{OH})_2$  content than the control portland cement paste. The incorporation of the RHA in concrete reduced its porosity and the  $\text{Ca}(\text{OH})_2$  amount in the interfacial zone; the width of the interfacial zone between the aggregate and the cement paste was also reduced compared with the control portland cement composite. However, the porosity in the interfacial zone of the rice-husk ash composite was higher than that of the silica fume composite. The incorporation of the RHA in the cement paste did not increase its compressive strength compared with that of the control. The higher compressive strength of the RHA concrete compared with that of the control is due probably to the reduced porosity, reduced  $\text{Ca}(\text{OH})_2$ , and reduced width of the interfacial zone between the paste and the aggregate.

**KEYWORDS:** compressive strength, concrete, DTA/TGA, hydration, image analysis, interfacial zone, paste, portland cement, rice-husk ash (RHA), XRD.

**Introduction**

Rice husk, an agricultural waste, constitutes about one fifth of the 500 million metric tons of rice produced annually in the world [1]. Due to the growing environmental concern, and the need to conserve energy and resources, efforts have been made to burn the husks at controlled temperature and atmosphere, and to utilize the ash so produced as a building material [1-14].

Rice-husk ash (RHA) is a very fine pozzolanic material [1,14] and its particle size and specific surface depend upon the burning conditions under which it is produced. In general, the average particle size ranges from 5 to 10  $\mu\text{m}$ , and the specific surface area ranges from 20 to 50  $\text{m}^2/\text{g}$ . A previous investigation [13] indicated that the rice-husk ash used in this study is highly pozzolanic, and can be used as a supplementary cementing material to produce high-performance concrete. The concrete incorporating 10% of the RHA as a cement replacement had somewhat higher compressive strength and higher resistance to chloride-ion penetration compared with the control portland cement concrete of the same water-to-cementitious materials ratio.

This paper presents an experimental study on the effects of the incorporation of rice-husk ash in cement paste and concrete on the cement hydration and the microstructure of the interfacial zone between the aggregate and paste. The influence on the compressive strength of concrete is discussed, and the results are compared with those obtained with concrete incorporating silica fume, and a control portland cement concrete.

TABLE 1  
Physical Properties and Chemical Analyses of the Cement, RHA, and Silica Fume

	ASTM Type I Cement	Rice husk ash	Silica Fume
<b>Physical Tests</b>			
Specific gravity	3.09	2.06	2.20
Fineness			
-passing 45 $\mu\text{m}$ , %	93.0	99.0	96.9
-specific surface, Blaine, $\text{m}^2/\text{kg}$	373	-	-
-nitrogen adsorption, $\text{m}^2/\text{g}$	-	38.9	26.1
Setting time, min.,			
-initial	135	-	-
Compressive strength of 51 mm cube, MPa			
-7-day	27.8	-	-
-28-day	39.1	-	-
Pozzolanic Activity Index, %	-	-	122.9
<b>Chemical Analyses, %</b>			
Silicon dioxide ( $\text{SiO}_2$ )	20.1	87.2	93.6
Aluminum oxide ( $\text{Al}_2\text{O}_3$ )	4.51	0.15	0.06
Ferric oxide ( $\text{Fe}_2\text{O}_3$ )	2.50	0.16	0.45
Calcium oxide ( $\text{CaO}$ )	61.3	0.55	0.50
Magnesium oxide ( $\text{MgO}$ )	3.13	0.35	0.67
Sodium oxide ( $\text{Na}_2\text{O}$ )	0.24	1.12	0.16
Potassium oxide ( $\text{K}_2\text{O}$ )	0.39	3.68	0.85
Phosphorous oxide ( $\text{P}_2\text{O}_5$ )	<0.9	0.50	0.09
Titanium oxide ( $\text{TiO}_2$ )	0.24	0.01	0.01
Sulphur oxide ( $\text{SO}_3$ )	4.04	0.24	0.32
Chlorides (Cl)	-	0.45	-
Carbon (C)	-	5.91	-
Loss on ignition	2.41	8.55	2.26
<b>Bogue Potential Compounds</b>			
Tricalcium silicate $\text{C}_3\text{S}$	51.3	-	-
Dicalcium silicate $\text{C}_2\text{S}$	19.0	-	-
Tricalcium aluminate $\text{C}_3\text{A}$	7.7	-	-
Tetracalcium aluminoferrite $\text{C}_4\text{AF}$	7.6	-	-

### Scope of Investigation

Hydration products, non-evaporable water and  $\text{Ca(OH)}_2$  contents of the RHA admixed cement paste were determined at the ages of 1, 7, 28, and 91 days using X-ray diffraction (XRD) and thermal analyses (DTA/TGA) methods. Unhydrated cement content in the specimens cured for 28 days were determined by analyzing backscattered electron images of the pastes. The effect of the incorporation of the RHA on the microstructure of the interfacial zone was studied by analyzing backscattered electron images of the polished samples of gap-graded concrete with a maximum aggregate size of 9.5 mm. The compressive strength of the RHA concrete composites was compared with that of the control portland cement and the silica fume composites.

### Materials

**Cement.** An ASTM Type I normal portland cement was used. Its physical properties and chemical composition are given in Table 1.

**Rice-Husk Ash (RHA).** The RHA used was a processed waste material incinerated at a controlled temperature and atmosphere. The chemical composition and physical properties of the RHA are also given in Table 1. It contains a carbon content of 5.91%, and is black in colour. Chemical analysis indicates that the material is principally composed of  $\text{SiO}_2$  (87.2%), and is also high in loss on ignition (8.55%). The ash contains a relatively high potassium content which originates mainly from the soil or due to the use of fertilizers.

The RHA has a specific gravity of 2.06. The particle size distribution of the material is shown in Fig. 1, together with that of the portland cement used in this study. The median particle size of the RHA is approximately 7  $\mu\text{m}$ , while that of the cement is approximately 13  $\mu\text{m}$ . The RHA, however, has an extremely high specific surface of 38.9  $\text{m}^2/\text{g}$  as determined by the nitrogen absorption technique, and is 1.5 times of that for the silica fume. Scanning electron microscopy (Fig. 2) shows that the material is very porous, thus explaining its high specific surface [1,8], and like that of cement, the particles of RHA are angular. X-ray diffraction

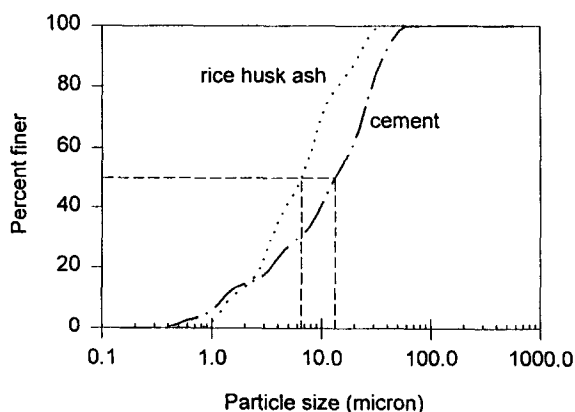


FIG. 1.  
Particle size distribution of the rice-husk ash and cement.

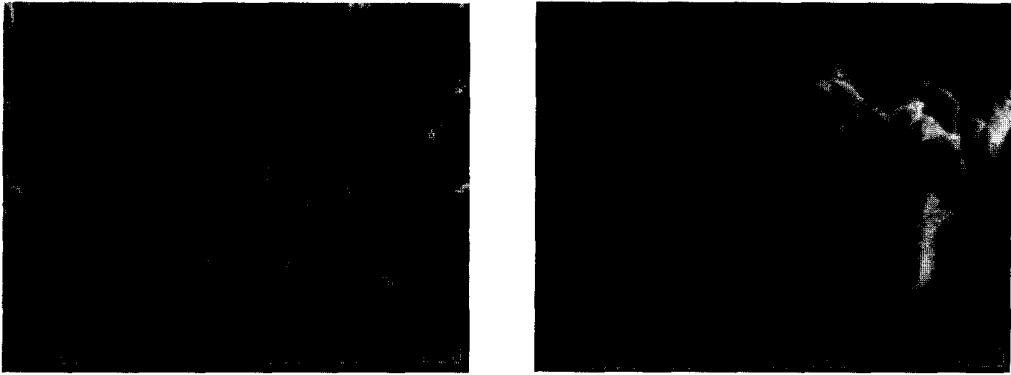


FIG. 2.

Scanning electron micrograph of the rice husk ash.

analysis (Fig. 3) indicates that the ash contains mainly amorphous materials with a small quantity of crystalline phases such as cristobalite (high-temperature phase of  $\text{SiO}_2$ ) and sylvite ( $\text{KCl}$ ), which is probably originated from the use of the fertilizers.

**Silica Fume (SF).** The silica fume used was a dry uncompacted powder. The chemical composition and physical properties of the silica fume are given in Table 1. The principal chemical component of the silica fume is also  $\text{SiO}_2$  (93.6%). It has a specific gravity of 2.2 and a specific surface area of approximately  $26.1 \text{ m}^2/\text{g}$ . X-ray diffraction analysis indicates that it contains mainly amorphous materials with a negligible quantity of crystallized quartz ( $\text{SiO}_2$ ) and silicon carbide ( $\text{SiC}$ ).

**Aggregate.** The coarse aggregate was a crushed limestone with a maximum nominal size of 19 mm, and the fine aggregate was local natural silica sand from the Ottawa area. Both the coarse

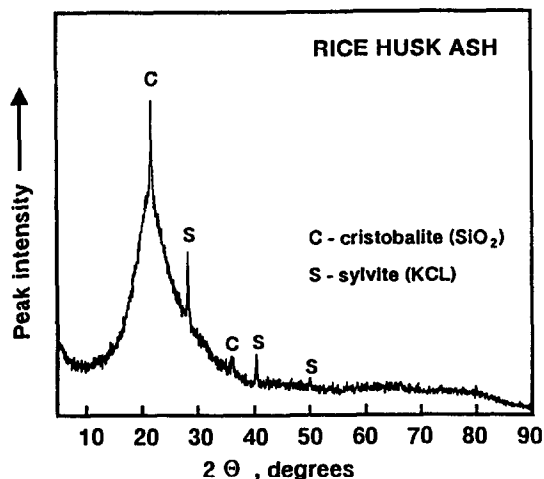


FIG. 3.

X-ray diffraction spectrum of the rice husk ash.

TABLE 2  
Grading of the Aggregates

Coarse aggregate		Fine aggregate	
Sieve size (mm)	Cumulative percentage retained	Sieve size (mm)	Cumulative Percentage retained
19.0	0.0	4.75	0.0
12.7	40.0	2.36	10.0
9.50	65.0	1.18	32.5
4.75	100.0	0.60	57.5
		0.30	80.0
		0.15	94.0
		pan	100.0

and fine aggregates were separated into different size fractions, and then recombined to a specified grading shown in Table 2. The coarse and fine aggregates had specific gravities of 2.69 and 2.70, and water absorption of 0.82 and 1.10% respectively.

**Superplasticizer.** A sulphonated, naphthalene formaldehyde condensate-based superplasticizer was used for the concrete mixtures and for the paste mixtures containing RHA and silica fume. The superplasticizer is a dark brown solution containing 42% solids.

### Mixture Proportions

The proportions of the paste and concrete mixtures are summarized in Tables 3 and 4, respectively; all the mixtures had a water-to-cementitious materials ratio of 0.30, and the superplasticizer was used to adjust the flow of the paste and the slump of the concrete.

### Preparation of Paste Specimens

For the compressive strength of the paste mixtures, fifteen  $50.8 \times 50.8 \times 50.8$ -mm cubes were cast in two layers, compacted on a vibrating table, and cured in a moist room at  $20 \pm 3^\circ\text{C}$  and

TABLE 3  
Mixture Proportions for Cement Paste Composite

Mix No.	RHA content (%)	Silica fume content (%)	W/C or W/C+RHA or W/C+SF	Quantities (kg)				
				Water*	Cement	RHA	Silica fume	SP**
PC0	0	0	0.30	1.65	5.50	0	0	0
PR10	10	-	0.30	1.66	4.95	0.55	-	0.017
PSF10	-	10	0.30	1.67	4.95	-	0.55	0.028

\* including the water in the superplasticizer

\*\* superplasticizer, naphthalene based

100% relative humidity until the time of testing. For the determination of the other properties of the pastes, cylinders, 30 × 50-mm in size, were prepared, and cured in the same manner as the cubes.

For determining the characteristics of the interfacial zone, composite specimens were made which had a water-to-cementitious materials ratio of 0.30 identical to that of the paste mixtures (Table 3). After the pastes were made, the aggregate of a single fraction (4.75-9.5 mm) was added, and hand mixed in the pastes. The reason for the above was that mechanical mixing of the materials would cause the break-up of the aggregate particles and this would result in difficulty in analyzing and interpreting the backscattered electron images of the interfacial zone. Test cylinders, 30 × 50-mm in size, were prepared and cured as described above.

### Preparation of Samples for XRD, DTA/TGA, and Image Analysis

Samples for XRD and DTA/TGA analyses were taken from acetone quenched solid pastes at prescribed ages and ground in acetone to arrest further hydration. This was followed by drying in a vacuum oven at 105°C for approximately two hours.

For backscattered electron image analysis, fragments were taken from the centre of 30 × 50-mm cylinder specimens at 28 days such that all surfaces were free of mould wall impression. Hydration was arrested by drying the samples in a vacuum oven at 50°C for approximately 24 hours. The dried samples were then embedded and vacuum impregnated in a low viscosity epoxy resin. After impregnation and curing of the epoxy, the specimens were lapped and polished. Alcohol was used as a lubricant and coolant for cutting and polishing to avoid further cement hydration and dissolution of hydration products. The polished specimens were coated with carbon for examination.

### Mixing of Concrete and Preparation of Concrete Specimens

The concrete was mixed in a laboratory counter-current mixer for a total of 5 min. The properties of the fresh concrete including slump, air content, and unit weight were determined, and are given in Table 5. Fifteen 102 × 203-mm cylinders were cast from each mixture, and compacted on a vibrating table in two layers. The specimens were left covered in the casting room at 20 ± 3°C for 24 hours then demoulded and cured in a moist-curing room until the time of testing in compression.

TABLE 4  
Mixture Proportions for Concrete

Mix No.	RHA content (%)	Silica fume content (%)	W/C or W/C+RHA or W/C+SF	Quantities (kg/m <sup>3</sup> )						
				Water*	Cement	RHA	Silica fume	Fine agg.	Coarse agg.	SP**
CC0	0	0	0.30	134.9	447.8	0	0	708	1153	6.9
CR10	10	-	0.30	134.8	403.2	44.8	-	699	1137	9.6
CSF10	-	10	0.30	134.9	406.6	-	45.2	706	1149	7.9

\* including the water in the superplasticizer

\*\* superplasticizer, naphthalene based

**TABLE 5**  
**Properties of Concrete**

Mix No.	Type of concrete	W/C or W/C+RHA or W/C+SF	Fresh Concrete				Hardened Concrete					
			Temperature (°C)	Slump (mm)	Unit weight (kg/m <sup>3</sup> )	Air content (%)	Unit weight (1-day) (kg/m <sup>3</sup> )	Compressive strength <sup>1</sup> (MPa)				
								1d	7d	28d	90d	180d
CC0	Control	0.30	25	150	2472	2.4	2467	41.4	52.1	61.0	70.6	76.5
CR10	10 % RHA	0.30	25	120	2458	2.4	2466	41.4	57.9	70.8	78.9	81.7
CSF10	10 % silica fume	0.30	25	110	2472	1.7	2471	44.4	64.8	78.9	77.8	80.8

\* average of three 102x203-mm cylinders.

### Testing

**X-Ray Diffraction Analysis.** Powder samples were scanned by a rotating-anode X-ray diffractometer using CuK $\alpha$  radiation at 55 kV and 180 mA and scanning from  $2\theta = 5-90^\circ$ . The data were analyzed using a search-match system of software.

**Thermal Analyses.** Thermal analyses of the prepared samples were conducted on a differential thermal analyzer DTA-50 and thermogravimetric analyzer TGA-50 operating under the following conditions:

Atmosphere:	dry N <sub>2</sub> gas
Flow rate:	40 mL/min
Temperature range:	21-900°C
Rate of temperature rise:	10°C/min
Sample weight:	15-18 mg

**Analysis of Backscattered Electron Images.** Analysis of backscattered electron images was conducted with a KONTRON-IBAS image analyzer coupled with an electron microprobe. Image analysis of the polished sections of composite samples was performed using backscattered electron images (BEI), obtained at an acceleration voltage of 20 kV and a beam current of 15 nano-ampere (nA).

The image analyzer was programmed for two main tasks:

- (a) to determine the unhydrated cement content of the paste,
- (b) to determine the porosity profile and Ca(OH)<sub>2</sub> content in the interfacial zone.

The choice of the magnification selected reflects a compromise between resolution of the phases and the need to obtain a representative sampling without undue effort. A magnification of 540 $\times$  was chosen for the analysis, the backscattered electron images were digitized into grey level images of 512  $\times$  512 pixels. therefore the geometric scale corresponds to approximately

<sup>1</sup>Rigaku X-ray diffractometer

<sup>2</sup>Fein-Marquart  $\mu$ PDSM software

<sup>3</sup>Shimadzu DTA/TGA 50

<sup>4</sup>JEOL JXA-733 microprobe

0.25  $\mu\text{m}/\text{pixel}$ . These conditions allow to resolve pores or grains of phases as small as 1  $\mu\text{m}$ . However, the full length of the field at 540 $\times$  is 128  $\mu\text{m}$  (i.e.,  $512 \times 0.25$ ). Therefore, at this magnification, the maximum size for the features, pores or grains is 128  $\mu\text{m}$ . The image analysis was performed with ten to twelve fields from each specimen. the general strategy for the routines is given in Appendix I.

**Compressive Strength.** Compressive strength of the concrete and paste specimens were determined according to ASTM C 39 and C 109, respectively. The results are given in Tables 5 and 6, respectively.

## Results and Discussion

### Characteristics of the Control, RHA, and Silica Fume Pastes.

*Hydration and reaction products.* Hydration and reaction products of the control, RHA, and silica fume pastes at the ages of 1, 7, 28, and 91 days were identified by X-ray diffraction and thermal analysis methods on powder samples prepared from acetone quenched paste specimens. Qualitative analyses of the paste mixtures show that calcium hydroxide [ $\text{Ca}(\text{OH})_2$ ] and calcium silicate hydrates [C-S-H] are the predominant product phases for all the three paste samples.

*Unhydrated cement content and porosity.* According to the image analysis, the control portland cement paste contained 22% unhydrated cement particles; the percentage of the unhydrated cement particles in the RHA and silica fume pastes was 18% and 20%, respectively, after 28 days of curing. The standard deviation of the analysis was 2.4, 2.5, and 1.6% for the control, the RHA, and the silica fume pastes, respectively. As the RHA was used as a 10% cement replacement, the reduction of unhydrated cement particles to 18% indicates a possible acceleration of the cement hydration in the presence of RHA, but this needs to be confirmed by additional research.

Figure 4 gives the weight loss for the pastes as a function of the time determined by drying the specimens in an oven at 105°C to a constant weight. The weight loss is an indication of the total porosity, while the rate of the weight loss is an indication of the relative size of the pores in the pastes. The porosity determined by this method includes all the gel and capillary pores as well as air voids. The results showed that the total porosity of the control, the RHA, and the silica fume pastes was similar, but the rate of the weight loss for the RHA and the silica fume pastes was slower than that of the control paste, indicating a refinement of the pore structure in the RHA and silica fume pastes.

TABLE 6  
Properties of the Pastes

Mix No.	Type of mixture	W/C or W/C+RHA or W/C+SF	Flow (%)	Unit weight ( $\text{kg}/\text{m}^3$ )	Compressive strength* (MPa)				
					1d	7d	28d	90d	180d
PC0	Control	0.30	116	2115	46.5	75.9	96.0	113.3	118.7
PR10	10 % RHA	0.30	115	2077	44.8	77.9	94.1	94.4	97.7
PSF10	10 % silica fume	0.30	100	2077	44.6	74.3	83.1	94.5	97.2

\* Average of three 51-mm cubes



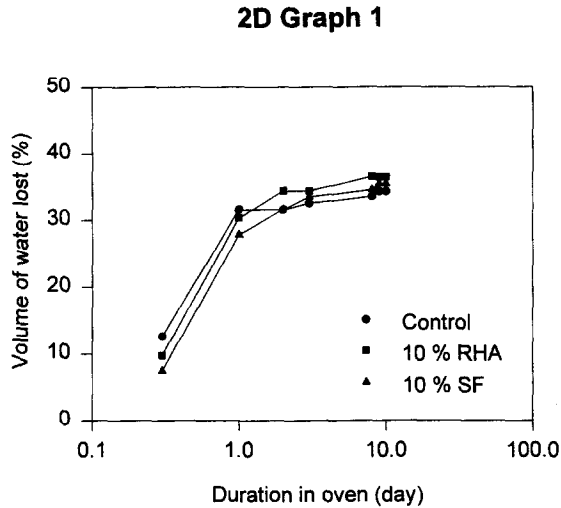


FIG. 4.

Weight loss of the pastes when dried in oven at 105°C, which is presented as volume of water lost relative to paste volume.

*Non-evaporable water and calcium hydroxide contents.* The results on the non-evaporable water (weight loss registered between 105 and 900°C) and  $\text{Ca}(\text{OH})_2$  content determined by TGA are presented in Figs. 5 and 6.

The results in Fig. 5 show that the RHA paste contained less non-evaporable water than the control paste, but more than the silica fume paste. At 91 days, the control, the RHA, and the silica fume pastes contained 14.1, 12.7, and 10.7% non-evaporable water, respectively. However, no conclusion can be drawn as to the degree of hydration of the different pastes based upon the above because C/S ratio and (C+S)/H of the C-S-H hydrates in these pastes are probably different due to the pozzolanic reactivity of the RHA or silica fume incorporated.

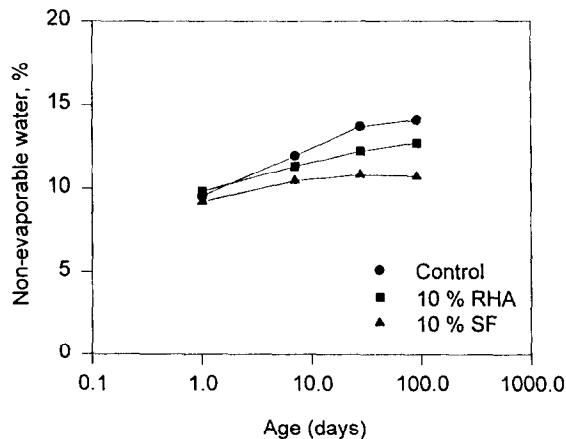


FIG. 5.

Non-evaporable water content in the pastes.

The results in Fig. 6 show that the RHA paste had lower  $\text{Ca}(\text{OH})_2$  content than the control paste at all ages. Compared with the silica fume paste, however, the RHA paste had similar  $\text{Ca}(\text{OH})_2$  content at 1 and 7 days, but higher values after 28 days. At 91 days, the control, the RHA, and the silica fume pastes contained 15.1, 8.2, and 5.3%  $\text{Ca}(\text{OH})_2$ , respectively.

The lower  $\text{Ca}(\text{OH})_2$  and the lower unhydrated cement contents discussed earlier for the RHA paste compared with the control paste clearly indicate the pozzolanic reactivity of the RHA. Compared with the silica fume, however, the reactivity of the RHA appears less significant at later ages, and this may be attributed to the difference in their particle characteristics.

**Compressive strength.** The compressive strength of the control, the RHA, and the silica fume pastes are given in Table 6, and illustrated in Fig. 7. The cement paste with 10% RHA had strength similar to that of the control paste up to 28 days, but lower values at 90 and 180 days. The strength of the RHA and the silica fume pastes were comparable. The strength tests at 1, 7, and 28 days were repeated three times and the results showed the same trend.

**Interfacial Zone Between the Paste and Aggregate.** The enhanced mechanical properties and reduced permeability of silica fume concrete is believed to be due to the reduction in the thickness of the interfacial zone between the aggregate and paste matrix [15-18]. Due to its extremely fine size and high pozzolanic reactivity, silica fume reduces the porosity, and also the preferential deposition of  $\text{Ca}(\text{OH})_2$  in the interfacial zone [19]. The rice-husk ash used in this study has a median particle size of about 7  $\mu\text{m}$ , which is somewhat finer than that of cement, but much coarser than that of silica fume (approximately 0.1  $\mu\text{m}$ ). From the particle size perspective, the RHA may not have as strong an effect on the reduction of porosity in the interfacial zone in concrete as the silica fume.

Figure 8 shows the porosity of the pastes as a function of the distance from the aggregate surface on test specimens cured for 28 days. From the figure, it can be seen that at 20  $\mu\text{m}$  from the aggregate surface, the porosity for the control, RHA, and SF samples was approximately 25, 18, and 10%, respectively; at 33  $\mu\text{m}$ , the porosity was approximately 17, 9, and 7%,

2D Graph 1

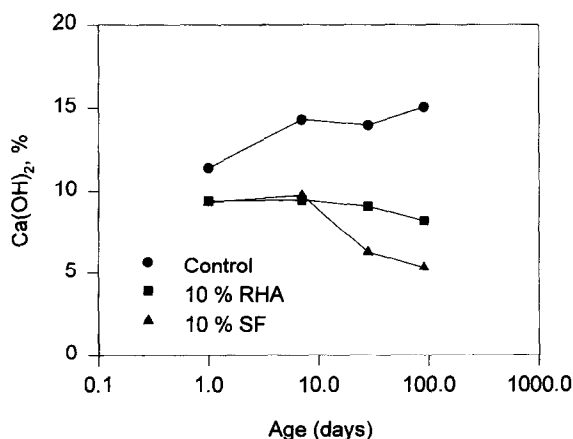


FIG. 6.  
Calcium hydroxide content in the pastes.

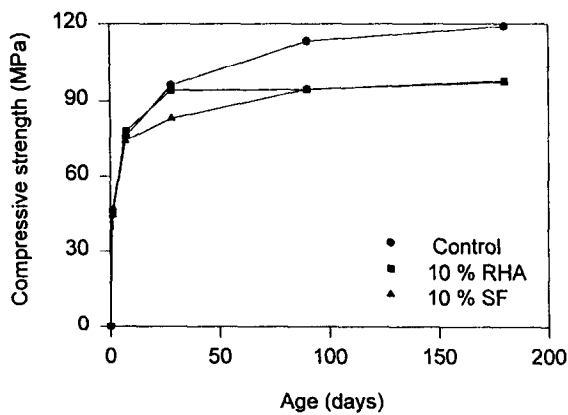


FIG. 7.  
Compressive strength of the pastes.

respectively, and at 43  $\mu\text{m}$ , the porosity was approximately 11, 5, and 7%, respectively. This indicates that the incorporation of the RHA reduced the porosity in the interfacial zone compared with that of the control portland cement composite. However, the porosity of the RHA composite in the first 30  $\mu\text{m}$  of the interfacial zone was higher than that of the silica fume composite, which may essentially be due to the coarser particle size of the RHA compared with that of the silica fume. Figure 8 also shows that the width of the interfacial zone, where the porosity is higher than that in the bulk paste, was approximately 60, 40, and 40  $\mu\text{m}$  for the control, RHA, and SF samples, respectively. The reduction of the width of the interfacial zone by the incorporation of the rice husk ash is probably similar to the effect of silica fume. The

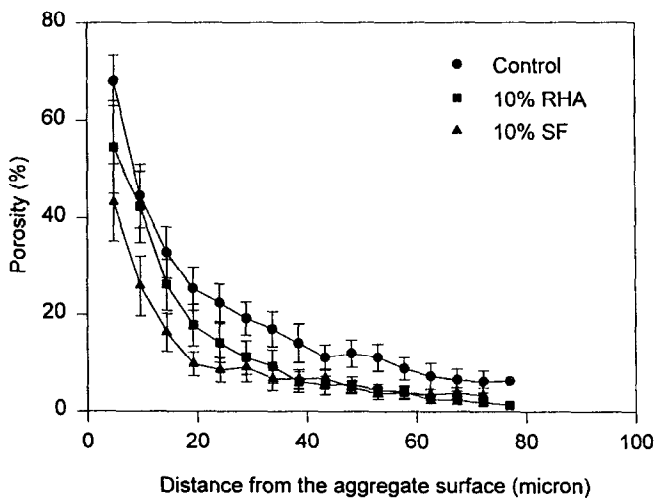


FIG. 8.  
Porosity profiles of the interfacial zone between aggregate and cement pastes (data presented are the average  $\pm$  one standard deviation).

analysis also showed a lower  $\text{Ca}(\text{OH})_2$  content in the interfacial zone for the RHA composite than that for the control one. Nilsen, Sandberg, and Folliard [20] also observed decreased relative concentration of  $\text{Ca}(\text{OH})_2$  in the interfacial zone with the replacement of cement by the RHA using quantitative X-ray diffraction analysis technique.

The reduction of porosity and  $\text{Ca}(\text{OH})_2$  content in the interfacial zone of the RHA composite observed might contribute to the enhancement of mechanical properties and the reduction of permeability of the concrete [13]. This effect, though different in magnitude, is probably similar to that of silica fume in concrete [19].

**Compressive Strength of Control, RHA, and Silica Fume Concretes.** The compressive strength development with age for the various concretes is presented in Table 5 and illustrated in Fig. 9. The RHA and the control concrete had similar one-day strengths, but the RHA concrete had somewhat higher strength than the control concrete thereafter up to 180 days. Compared with the silica fume concrete, the compressive strength of the RHA concrete was lower up to 28 days, but similar at 90 and 180 days.

Generally, concrete can be considered as a composite material with the coarse aggregate embedded in the mortar matrix, and the sand embedded in the cement paste. For normal weight aggregate concrete, the interfacial zone between the aggregate and cement paste is usually the weakest part of the concrete due to its higher w/c and porosity; this zone therefore, controls the strength and to a large extent the permeability of the concrete.

Comparing the strength of the RHA concrete and the corresponding paste incorporating RHA, it appears that the rice-husk ash contributed to the strength of the paste and the concrete in different ways and to a different extent. Even though the strength of the RHA paste was similar to or lower than the control paste, the strength of the RHA concrete was higher than that of the control concrete, indicating that the increase in the strength of the RHA concrete may be primarily due to the improvement of the interfacial zone between the aggregate and the binder. Similar results have been reported by others for the silica fume pastes and concretes [18].

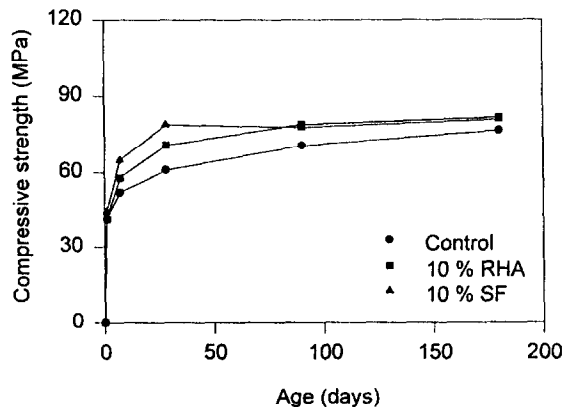


FIG. 9  
Compressive strength development of concretes versus age.

Because of the larger particle size, the magnitude of such an effect of the RHA is probably less than that of the silica fume; data on the compressive strength of the pastes and the concretes as well as the porosity profile in the interfacial zone confirmed this.

### Conclusions

Based on the limited experiments, the following conclusions may be drawn:

1. As for ordinary portland cement paste, the calcium hydroxide  $[\text{Ca}(\text{OH})_2]$  and calcium silicate hydrates  $[\text{C-S-H}]$  were the major hydration and reaction products in the RHA paste. Because of the pozzolanic reaction, the paste incorporating RHA had lower  $\text{Ca}(\text{OH})_2$  content than the control portland cement paste.
2. The incorporation of the RHA in concrete reduced the porosity and the  $\text{Ca}(\text{OH})_2$  amount in the interfacial zone; the width of the interfacial zone between the aggregate and the cement paste compared with the control portland cement composite was also reduced. However, the porosity of the rice-husk ash composite in the interfacial zone was higher than that of the silica fume composite.
3. The cement paste incorporating RHA did not show any increase in the compressive strength compared with that of the control portland cement paste. The higher compressive strength of the RHA concrete compared with that of the control concrete is due probably to its reduced porosity, reduced  $\text{Ca}(\text{OH})_2$  content, and the reduced width of the interfacial zone between the paste and the aggregate.

### Acknowledgments

The authors acknowledge the assistance of: R. Chevrier for the laboratory work on concrete; M. Beaulne for the preparation of polished samples for image analysis, and P. Carriere for the XRD analysis.

### References

1. Mehta, P. K., "Rice Husk Ash-A Unique Supplementary Cementing Material," Proceedings of the International Symposium on Advances in Concrete Technology, ed. V. M. Malhotra, Athens, Greece, May 1992, pp. 407-430.
2. Cook, D.J., Pama, R. P., and Damer, S. A., "The behaviour of Concrete and Cement Paste Containing Rice Husk Ash," Conference Proceedings on Hydraulic Cement Paste, Cement & Concrete Association, London, 1976.
3. Mehta, P.K. and Pitt N., "Energy and Industrial Materials from Crop Residues," *Resource Recovery and Conservation*, 2, 1976, pp. 23-38.
4. Mehta, P.K., "Properties of Blended Cements Made from Rice Husk Ash," *ACI Journal*, Sept. 1977, pp. 440-442.
5. Manmohan, D. and Mehta, P.K., "Influence of Pozzolanic, Slag, and Chemical Admixtures on Pore Size Distribution and Permeability of Hardened Cement Pastes," *Cement, Concrete, and Aggregates*, Vol. 3, No.1, Summer 1981, pp.63-67.
6. Yamamoto, Y. and Lakho, S. M., "Production and Utilization of Active Rice Husk Ash As A Substitute for Cement," Proceedings of JSCE, No. 322, June 1982, pp. 157-166.

7. James, J. and Rao S., "Characterization of Silica in Rice Husk Ash," *Ceramic Bulletin*, Vol. 65, No. 8, 1986, pp. 1177-1180.
8. Hwang, C.-L. and Wu, D.-S., "Properties of Cement Paste Containing Rice Husk Ash," ACI SP114-35, Proceedings of the Third CANMET/ACI International Conference on Fly Ash, Silica Fume, Slag and Natural Pozzolans in Concrete, Trondheim, Norway, ed. V. M. Malhotra, 1989, pp. 733-762.
9. Boateng, A.A. and Skeete, D.A., "Incineration of Rice Hull for Use as a Cementitious Material: The Guyana Experience," *Cement and Concrete Research*, Vol. 20, 1990, pp. 795-802.
10. Singh, N.B., Sarvahi, R., Singh, S.P., and Shukla, A.K., "Hydration Studies of Rice Husk Ash Blended White Portland Cement," *Advances in Cement Research*, Vol. 6, No. 21, Jan. 1994, pp. 13-18.
11. Mehta, P. K., "Siliceous Ashes and Hydraulic Cements Prepared Therefrom," Belgium Patent 802909, July 1973, U.S. Patent 4105459, August 1978.
12. Pitt, N., "Process for preparation of siliceous ashes," U.S. Patent 3959007, May 1976.
13. Zhang, M. H. and Malhotra, V. M., "High-Performance Concrete Incorporating Rice Husk Ash as a supplementary Cementing Materials," accepted for publication in the *ACI Materials Journal*.
14. Cook, D. J., "Rice Husk Ash," Concrete Technology and Design: Vol. 3, Cement Replacement Materials, Ed. R.N. Swamy, published by Surrey University Press, 1986, pp.171-196.
15. Goldman, A. and Bentur, A., "Bond Effects in High-Strength Silica-Fume Concretes," *ACI Materials Journal*, Sept.-Oct. 1989, pp. 440-447.
16. Goldman, A. and Bentur, A., "The influence of Microfillers on Enhancement of Concrete Strength," *Cement and Concrete Research*, Vol. 23, 1993, pp. 962-972.
17. Bentur, A. Cohen, M.D., "Effect of Condensed Silica Fume on the Microstructure of the Interfacial Zone in Portland Cement Mortars," *Journal of American Ceramic Society*, Vol. 70, 1987, pp. 738-743.
18. Bentur, A., Goldman, A., and Cohen, M.D., "The contribution of the Interfacial Zone to the Strength of High Quality Silica Fume Concretes," presented at the Materials Research Society Annual Meeting, 1987, Symposium on Bonding in Cement Composites.
19. Scrivener, K. L., Bentur, A. and Pratt, P. L., "Quantitative Characterization of the Transition Zone in High Strength Concretes," *Advances in Cement Research*, Vol. 1 No. 4, Oct. 1988, pp. 230-237.
20. Nilsen, U., Sandberg, P., and Folliard, K., "Influence of Mineral Admixtures on the Transition Zone in Concrete," *Interfaces in Cementitious Composites*, Proceedings of the International Conference held by RILEM, Toulouse, France, Oct. 21-23, 1992, ed. J. C. Maso, published by E & FN Spon, London, pp. 65-70.
21. Scrivener, K. L. and Gartner, E. M., "Microstructural gradients in cement paste around aggregate particles," Bonding in Cementitious Composites, Symposium Proceedings of Material Research Society, Vol. 114, Pittsburgh, 1988, eds. S. Mindess and S. P. Shah, pp. 77-85.
22. Scrivener, K. L. and Pratt, P. L., "The Characterization and Quantification of Cement and Concrete Microstructures," From Materials Science to Construction Materials Engineering, Proceedings of the 1st International RILEM Congress, Paris, 1987, Editor: J. C. Maso, published by Chapman & Hall, 1987, pp. 466-471.

## Appendix I

The image analysis routine for the determination of unhydrated cement content consisted of selecting an area randomly in the paste and segmenting the digitized backscattered electron image to make two binary images, one for the unhydrated cement and another for the total field. Small artifacts and noise were eliminated from the binary images by scraping away all features smaller than five square pixels. The total area in each clean binary image was then measured. The unhydrated cement content was calculated with reference to the total area of the field. A series of control variables was allowed to select another field into the paste and iterate the

procedure for as many images as desired. At the end, the image analysis program accumulated the area for the pores and for the unhydrated cement in all selected fields, then calculated the percentages with reference to the total area of all the fields. In this study 12 fields were selected for the analysis for each sample.

The image analysis routine for the determination of porosity and  $\text{Ca(OH)}_2$  content in the interfacial zone consisted of selecting a field showing the interface between the paste and the aggregate. The microprobe goniometers and scan-rotation controls were used to place the interface in a vertical position and as far to the left border of the image. A white line was manually drawn on the digitized backscattered electron image following the contour of the aggregate. The program used this line to make a  $4.8\text{ }\mu\text{m}$ -width band with the same contour of the interface from the grey-level image. The porosity or  $\text{Ca(OH)}_2$  was determined within this band using a similar image analysis strategy as the one described above, and was calculated with reference to the total area of the band. The program iterated moving the band to the right of the original grey image by one step equal to the band-width, and repeating measurements. The program was made to break the iteration loop as soon as the right-most border of the band reached the right border of the original grey image. This allowed to have all porosity calculated based on the same band-area. Ten fields were analyzed for each sample to obtain the porosity or  $\text{Ca(OH)}_2$  content.